

## Comparison of dust emissions, transport, and deposition between the Taklimakan Desert and Gobi Desert from 2007 to 2011

CHEN SiYu<sup>1</sup>, HUANG JianPing<sup>1\*</sup>, LI JingXin<sup>2</sup>, JIA Rui<sup>1</sup>, JIANG NanXuan<sup>1</sup>, KANG LiTai<sup>1</sup>, MA XiaoJun<sup>1</sup> & XIE TingTing<sup>1</sup>

<sup>1</sup> Lanzhou University, College of Atmospheric Sciences, Lanzhou 730000, China;

<sup>2</sup> Chinese Academy of Meteorological Sciences, Institute of Climate System (Polar Meteorology), State Key Laboratory of Severe Weather, Beijing 100081, China

Received January 9, 2017; accepted May 10, 2017; published online June 12, 2017

**Abstract** The Taklimakan Desert (TD) and Gobi Desert (GD) are two of the most important dust sources in East Asia, and have important impact on energy budgets, ecosystems and water cycles at regional and even global scales. To investigate the contribution of the TD and the GD to dust concentrations in East Asia as a whole, dust emissions, transport, and deposition over the TD and the GD in different seasons from 2007 to 2011 were systematically compared, based on the Weather Research and Forecasting model coupled with Chemistry (WRF-Chem). Dust emissions, uplift, and long-range transport related to these two dust source regions were markedly different due to differences in topography, elevation, thermal conditions, and atmospheric circulation. Specifically, the topography of the GD is relatively flat, and at a high elevation, and the area is under the influence of two jet streams at high altitudes, resulting in high wind speeds in the upper atmosphere. Deep convective mixing enables the descending branch of jet streams to continuously transport momentum downward to the mid-troposphere, leading to enhanced wind speeds in the lower troposphere over the GD which favors the vertical uplift of the GD dust particles. Therefore, the GD dust was very likely to be transported under the effect of strong westerly jets, and thus played the most important role in contributing to dust concentrations in East Asia. Approximately 35% and 31% of dust emitted from the GD transported to remote areas in East Asia in spring and summer, respectively. The TD has the highest dust emission capabilities in East Asia, with emissions of about  $70.54 \text{ Tg yr}^{-1}$  in spring, accounting for 42% of the total dust emissions in East Asia. However, the TD is located in the Tarim Basin and surrounded by mountains on three sides. Furthermore, the dominant surface wind direction is eastward and the average wind speed at high altitudes is relatively small over the TD. As a result, the TD dust particles are not easily transported outside the Tarim Basin, such that most of the dust particles are re-deposited after uplift, at a total deposition rate of about  $40 \text{ g m}^{-2}$ . It is only when the TD dust particles are uplifted above 4 km, and entrained in westerlies that they begin to undergo a long-range transport. Therefore, the contribution of the TD dust to East Asian dust concentrations was relatively small. Only 25% and 23% of the TD dust was transported to remote areas over East Asia in spring and summer, respectively.

**Keywords** East Asian dust, WRF-Chem model, Taklimakan Desert Dust, Gobi Desert Dust, Dust emissions, Dust transport, Dust deposition

**Citation:** Chen S Y, Huang J P, Li J X, Jia R, Jiang N X, Kang L T, Ma X J, Xie T T. 2017. Comparison of dust emissions, transport, and deposition between the Taklimakan Desert and Gobi Desert from 2007 to 2011. *Science China Earth Sciences*, 60: 1338–1355, doi: 10.1007/s11430-016-9051-0

### 1. Introduction

Dust aerosols are the main component of tropospheric

aerosols. As one of the most significant factors impacting climate change and energy budgets in the Earth system (Huang et al., 2006a, 2010; Fu et al., 2009; Zhang et al., 2009a, 2009b; Wang et al., 2010; Ge et al., 2010; Jia et al., 2015), it can not only alter radiative budget directly through

\* Corresponding author (email: hjp@lzu.edu.cn)

scattering and absorbing solar radiation, but also indirectly change clouds' albedo and life span through impacting cloud condensation nucleus and ice nucleus and thus further affecting precipitation efficiency (Huang et al., 2006b, 2011, 2014; Qian et al., 2009; Yue et al., 2010, 2013; Chen et al., 2014b). With its high dust emissions and wide diffusion range, East Asia is a major dust source, contributing large quantities of dust particles to the global dust mass loading (Zhang et al., 2003; Wang et al., 2012). Approximately 600 Tg of East Asian dust was ejected into the atmosphere annually, where about 30% was re-deposited in desert regions, 20% transported to inland areas in China, and the remaining 50% was transported over long distances to Korea, Japan, the Pacific, and across the Pacific to America, Canada and even as far as Greenland (Huang et al., 2008; Kim, 2008; Eguchi et al., 2009; Wang et al., 2016; Kang et al., 2016; Kang and Chen, 2017; Chen et al., 2013, 2017). Such high dust loadings over East Asia have significant impact on the environment and climate change at both local and global scales.

The Taklimakan Desert (TD) and Gobi Desert (GD) are two of the most important dust sources in Asia (Sun et al., 2001; Uno et al., 2008; Zhang B et al., 2008). Located in the central Tarim Basin (Figure 1), the TD covers an area of approximately 337600 km<sup>2</sup>, making it the largest desert in China and the second largest drifting desert in the world. The TD is surrounded by mountains on three sides: south of the Kunlun Mountains, north of the Tianshan Mountains, and east of the Pamirs Plateau. It is about 1000 km long from west to east and 400 km wide from north to south. As a desert in a warm temperate zone, the annual precipitation in the TD is no more than 100 mm (4–5 mm minimum), while the average evaporation is up to 2500–3400 mm. In addition, vegetation

in the TD is extremely scarce. The GD covers parts of northern and northwestern China and southern Mongolia, and is located to the east of the TD, surrounded by the Altai Mountains, Mongolian Prairie, Hexi Corridor, and the Qinghai-Tibet Plateau. As a plateau desert (the altitude of the GD is about 910–1520 m), temperatures in the GD are low but highly variable with an annual average of about -2.5°C but the peak of up to 35°C. The annual average precipitation over the GD is quite low at approximately 194 mm/year, as the Himalayas form a barrier that prevents the transport of moist air from the Indian Ocean.

In recent years, numerous studies related to the TD dust have been reported, including discussions on temporal and spatial variation (Gong et al., 2003; Ge et al., 2014), dust emissions (Zhang et al., 2003; Shao et al., 2011; Chen et al., 2014a), long distance transport (Uno et al., 2008; Huang et al., 2007, 2008; Zhang B et al., 2008), and radiative forcing characteristics (Su et al., 2008; Huang et al., 2009, 2012). However, studies on the GD dust are limited and have generally concentrated on springtime characteristics. Sun et al. (2001) showed that the GD was also a major dust source using the long-term observation records. Shao et al. (2003) found that dust emissions over the GD are intense. The dust emission flux can reach up to 1.6–4.3 t(km<sup>2</sup>d)<sup>-1</sup> in Loess Plateau areas, having impacts on most inland regions in China based on the real-time prediction of dust storms in the numerical model. Zhao et al. (2004) reported the dominant factors affecting dust storm frequency in central and western Inner Mongolia using 40-year meteorological records including surface winds, land surface conditions, the polar vortex area index in the Northern Hemisphere, and the polar vortex intensity index in the Asian Northern Hemisphere. Using Cloud-Aerosol Lidar and Infrared Pathfinder Satellite Observation (CALIPSO) retrievals, Huang et al. (2008) found that dust events are frequent, but blowing sand occurs primarily over the TD, while the frequency of dust storms is low but intense over the GD. Large quantities of dust particles are lifted to an altitude of 9 km, and may then be transported over long distances to eastern China and even the Pacific.

However, questions remain about the differences in dust emissions, transport and precipitation between the TD and the GD, and what results in such differences. In addition, there are uncertainties surrounding the contributions of the TD and the GD to East Asian dust. We analyze and compare the differences in dust emission, transport and wet/dry deposition over the TD and the GD in different seasons from 2007 to 2011 based on the WRF-Chem model (Weather Research and Forecasting coupled with Chemistry, hereinafter referred to as WRF-Chem), combined with satellite remote sensing data. We comprehensively attribute the reasons for these differences, and focus on the contributions of the two main sources of dust over East Asia in the study.

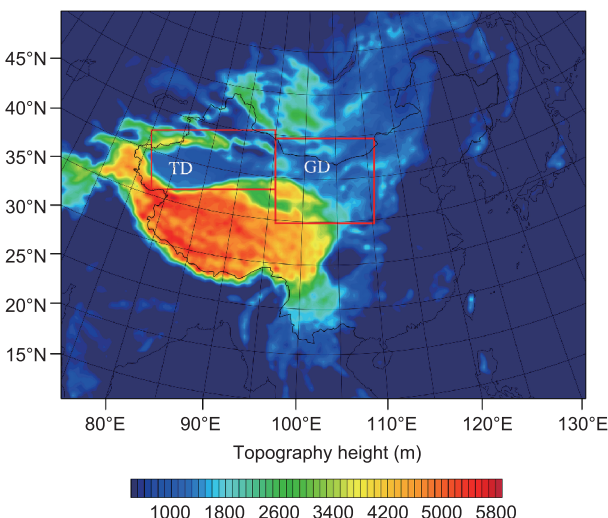


**Figure 1** Modeling domain and the spatial distribution of topography height. The red boxes represent the Taklimakan Desert (TD) and the Gobi Desert (GD) and were used for further analysis.

## 2. Model and observations

### 2.1 WRF-Chem model

The WRF-Chem model is a well-developed air quality model. Various schemes are coupled within the WRF-Chem model, such as gas-phase chemical mechanism, photolysis schemes, and aerosol mechanism. These schemes incorporate treatment of aerosol emissions, formation, transport (including advection, diffusion, and convection processes), wet/dry deposition, and radiation. Compared with other numerical models, the advantage of WRF-Chem lies in its completely online coupling between meteorological conditions and atmospheric chemistry at high temporal and spatial resolution, and can be a good indicator of feedback between aerosol and meteorological fields (Grell et al., 2005).

The Model Aerosol Dynamics Model for Europe (MADE), with the secondary organic aerosol model (SORGAM) (referred to as MADE/SORGAM), and the regional acid deposition model 2 photochemical reaction mechanism were implemented in the WRF-Chem model (Grell et al., 2005) in the study. The MADE/SORGAM model used three lognormal distribution modes (Aiken, accumulation and coarse, hereinafter referred to as 3-mode) to describe aerosol size distributions. The description of aerosol optical characteristics is detailed by Fast et al. (2006).

According to different hypotheses and simplified methods (Zender et al., 2003), there are three categories of dust emission schemes: (1) empirical dust emission schemes; (2) schemes based on simplified physical processes; (3) and schemes based on detailed microphysical processes. The GOCART (Georgia Tech/Goddard Global Ozone Chemistry Aerosol Radiation and Transport) scheme calculates dust fluxes for each dust particle bin according to the empirical formula of vertical dust flux and friction velocity, which has been widely applied to dust emissions at regional and global scales (Ginoux et al., 2001, 2004; Huneeus et al., 2010), particularly in Africa (Cavazos-Guerra and Todd, 2012) and North America (Zhao et al., 2010, 2013). The GOCART scheme is capable of simulating dust emissions at regional and global scales (Huneeus et al., 2010). Cavazos-Guerra and Todd (2012) used the GOCART dust scheme within the WRF-Chem model to simulate dust emissions over the Sahara desert during the West African monsoon period. By comparing with various ground-based and satellite data, they found that the scheme could reproduce the main characteristics of Saharan dust emissions well. Weaver et al. (2002) used the GOCART scheme coupled with a radiation transfer model to calculate the short and long-wave radiative forcing of Saharan dust and found good agreement with satellite observations. Zhao et al. (2010) adopted two dust schemes (GOCART and DUSTTRAN) and two aerosol modules (MADE/SORGAM and MOSAIC) in the WRF-Chem

model to investigate their uncertainties in the simulation of North African dust and its radiative forcing effects. It was shown that the two categories of dust emission schemes were relatively consistent in their representation of the temporal and spatial characteristics of dust emissions, but showed substantial differences in dust emission fluxes in local simulations. In addition, the GOCART scheme cannot only capture the temporal and spatial variation in dust emissions and concentrations in dust source regions over East Asia, but can also reproduce the observed dust concentrations in both the vicinity of dust sources and remote regions (Chen et al., 2013, 2014a, 2017). In addition, Cheng et al. (2012) found that simulations based on the GOCART scheme show good agreement with AERONET observations in China. The GOCART dust emission scheme calculates the dust emission flux  $G$  as follows:

$$G = CSs_p u_{10m}^2 (u_{10m} - u_t), \quad (1)$$

where  $C(\mu\text{g s}^{-2}\text{m}^{-5})$  is the dust emission factor, a highly variable empirical constant, with large uncertainties, that generally needs to be tuned according to satellite retrievals. We compared and verified simulation results with aerosol optical depth (AOD) from MODIS and Multi-angle Imaging SpectroRadiometer (MISR) retrievals over East Asia from 2007 to 2011, and found that the dust emissions well simulated the temporal and spatial distribution characteristics of dust aerosols over dust source regions and surrounding areas when the dust emission factor  $C=1 \mu\text{g s}^{-2}\text{m}^{-5}$  (Chen et al., 2014b). The dust source function  $S$  is based on topography combined with surface parameters such as vegetation and snow cover to limit the dust emission range in the simulation domain. It quantitatively characterizes the potential dust source regions in a grid. Figure 2 shows that the soil erodibility over East Asia used in the GOCART dust emission scheme can reproduce potential dust sources, having good agreement with

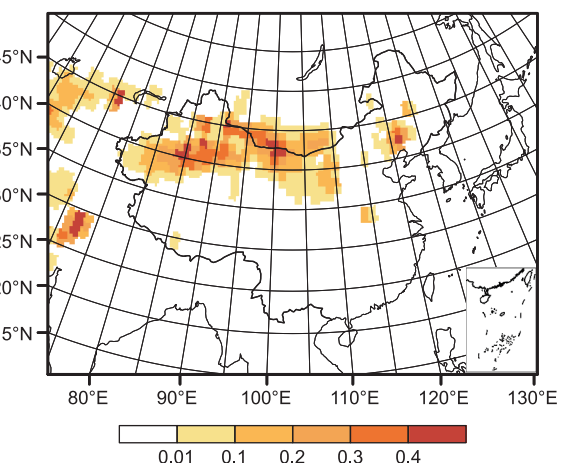


**Figure 2** The spatial distribution of soil erodibility in East Asia used in the GOCART dust emission, based on the WRF-Chem model.

desert distribution are achieved over East Asia (Nakano et al., 2004; Kanayama et al., 2005). Dust source regions are mainly distributed in northwestern China and in the vicinity of the Sino-Mongolian border. The TD and the GD are two of the largest deserts in these source regions, located in the south of Xinjiang Region and Mongolia, respectively. The TD is dominated by sand particles, while the GD is a mixture of mostly sand, sandy silt and clay (Figures are not shown). Thus, the magnitude of the dust source function over the TD is generally higher than that of the GD.  $u_{10m}$  is the mean horizontal wind speed at 10m;  $u_t$  is the threshold velocity at 10m, which is a function of particle size, air density and soil moisture. Ginoux et al. (2004) suggested that  $u_t \approx u_{*t}$ , where  $u_{*t}$  is the threshold friction velocity, calculated using the formula of Marticorena and Bergametti (1995) with consideration of the effects of soil moisture. The formula for  $u_t$  is as follows:

$$u_t = \begin{cases} A \sqrt{\frac{\rho_p - \rho_a}{\rho_a}} g \Phi_p (1.2 + 0.2 \log_{10} w) & \text{if } w < 0.5, \\ \infty & \text{otherwise,} \end{cases} \quad (2)$$

where  $A$  is the particle size ( $A=6.5$ );  $\rho_p$  and  $\rho_a$  are the particle and the air density, respectively;  $\Phi_p$  is the particle diameter;  $w$  is the soil moisture content, which depends on such factors as precipitation, evaporation and the water retention capacity of the soil, varying from 0.001 to 1, with values of above 0.5 after rain. Belly (1964) and Pye (1989) reported that the main factor in determining the magnitude of  $u_t$  is the interaction force among particles, which correlated with particle size and soil moisture. Shen et al. (2005) found that  $u_t$  increased with the increasing soil moisture and vegetation cover using Shao schemes combined with observations in Dunhuang. However, the dust source regions in East Asia are mainly located in the mid-latitude at altitude above 1500m where the annual precipitation is quite low. Furthermore, most of the dust events occurred in the dry and less rainy spring season. Therefore, the soil moisture content has little impact on dust emissions.

The configuration, initial and boundary conditions were the same as those used by Chen et al. (2014a, 2017). The Noah land surface module (Chen and Dudhia, 2001), Yonsei University (YSU) planetary boundary layer scheme (Hong et al., 2006), Kain-Fritsch cumulus scheme (Kain, 2004), Morrison two-moment microphysics scheme (Morrison et al., 2005), and RRTMG long and short-wave radiation scheme (Zhao et al., 2010) were used in the simulation. Anthropogenic emissions of CO, NO<sub>x</sub>, SO<sub>x</sub>, organic carbon, black carbon, volatile organic compounds and some anthropogenic aerosols were also taken into consideration. The initial meteorological fields and lateral boundary conditions were provided by the National Center for Environmental Prediction final analysis (NCEP/FNL) datasets with 1° horizontal resolution at 6h temporal intervals. The WRF-Chem model simulation was configured at 36km horizontal resolution with 35 vertical

layers up to 100 hPa. The domain covers the entirety of East Asia with 138×187 grid points (10.7–59.8°N, 51.6–154.4°E; see Figure 1). The simulation was conducted from June 1, 2006 to December 31, 2011. To avoid uncertainties surrounding the instability of simulation results shortly after model initialization, only the simulation results from January 1, 2007 to December 31, 2011 (hereafter referred to as the simulation period) were used in this analysis.

## 2.2 MISR Satellite Observations

The MISR, which was launched with the sun-synchronous polar-orbiting satellite Terra satellite, can view the sunlit Earth at the same point in nine widely spaced angles simultaneously (0°, ±26.1°, ±45.6°, ±60.0°, ±70.5°) with a swath width of 360km, in four spectral bands (446, 558, 672, and 866nm) (Martonchik et al., 2002, 2004). Because MISR obtains observational information at different angles to determine information at the surface, it can effectively remove the contribution of solar radiation reflected by the ground. Thus it has few limitations caused by the surface types, and this unique design enables it to retrieve aerosol properties over highly reflective surfaces, such as deserts (Diner et al., 2005, 2012; Kahn and Gaitley, 2015; Tesfaye et al., 2011; Zhang and Reid, 2010). Research has shown that AOD retrieved from MISR is in good agreement with ground-based observations in China (Cheng et al., 2012). The MISR aerosol product was used to evaluate the simulated AOD over East Asia in this study.

## 3. Results

### 3.1 WRF-Chem Evaluations

Previous work on validation of the WRF-Chem model coupled with the GOCART dust emission scheme has focused on North America, and Africa (Zhao et al., 2010). Large discrepancies have been reported in the simulation of dust over East Asia based on the WRF-Chem model, suggesting that knowledge gaps still exist for this region. Chen et al. (2014a, 2017) investigated the capability of the WRF-Chem model for the simulation of dust emissions over East Asia by comparison with various advanced ground observations and satellite retrievals. The results showed that the WRF-Chem model can reproduce the temporal and spatial characteristics of meteorological fields and dust concentrations over East Asia well, particularly for the vertical structure of dust in dust source regions, which provided confidence in further investigations of dust emissions, long-range transport, and deposition over the TD and the GD. In this study, we further compared the seasonal variation in the simulated wind field at 500hPa and AOD over East Asia with NCEP/FNL reanalysis data and MISR retrievals, respectively.

Figure 3 shows the spatial distribution of wind fields at

500 hPa from the NCEP/FNL reanalysis data and the WRF-Chem model in different seasons from 2007 to 2011. To nudge the simulation results to better reflecting the real atmo-

spheric large-scale circulation fields, the simulated horizontal and vertical wind components and the temperature fields above the planetary boundary layer were constrained to

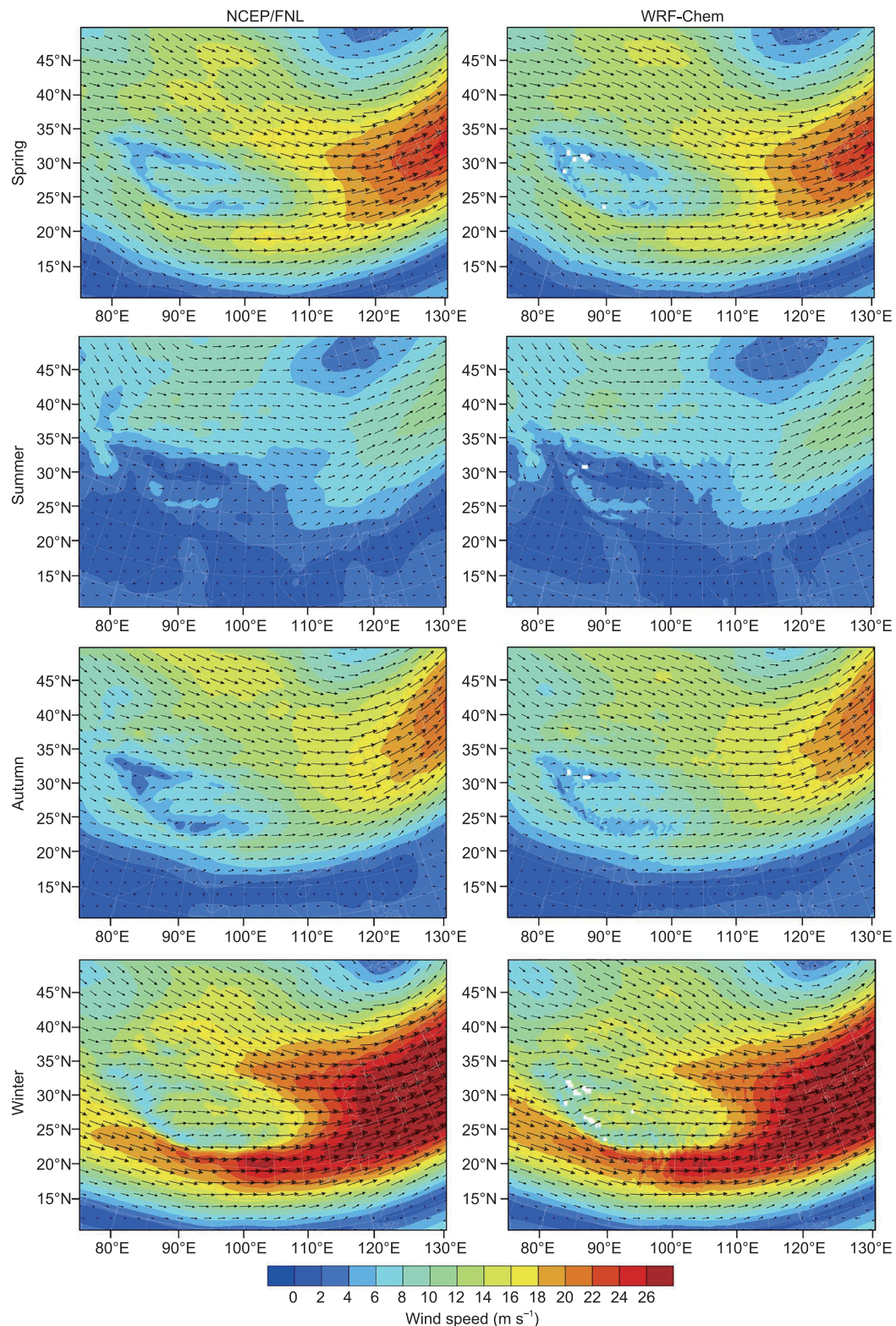


**Figure 3** Seasonal average wind fields at 500 hPa in 2007–2011 from NCEP/FNL data (left) and WRF-Chem simulations (right). Arrows represent the wind vector at 500 hPa.

NCEP/FNL datasets taken every six hours in the domain. Therefore, the simulated meteorological fields and reanalysis data were in good agreement. The WRF-Chem model reproduced the wind fields at 500hPa well. Specifically, the positions and intensities of the subtropical westerly jet and the subarctic westerly jet in the WRF-Chem model were consistent with those from NCEP/FNL data. The westerlies dominated most of the East Asian regions and wind speeds exhibited had obvious seasonal variations. The wind speeds at 500hPa were large in spring and winter. Due to the topographic blocking by the Tibetan Plateau (TP), the westerly air current flows were diverted into two branches around the plateau by north and south, which converged and produced larger wind speeds in the northeast of the TP, particularly in winter. Wind speeds at 500hPa were smallest in summer and the whole westerly jet moved northward to the north of the TP. The spatial distribution of temperature fields at 500hPa from the WRF-Chem simulation was also compared with those from the NCEP/FNL reanalysis data (Figures are not shown). These results demonstrate that the WRF-Chem model can reproduce the locations, shapes and depths of temperature troughs and ridge at 500hPa over East Asia well (Figures are not shown).

To verify the performance of the WRF-Chem model for dust aerosol optical characteristics over East Asia during the simulation period, the spatial distributions of seasonal AOD at 550nm during 2007–2011 from MISR satellite retrievals and WRF-Chem simulations were shown in Figure 4. To better match the observations, the model results were sampled at the overpass time of the MISR retrievals. Results showed that the large MISR AOD centers were located in the TD and the GD, with values larger than 0.45 in spring and summer. There were also high-value centers of AOD in eastern China and the Sichuan Basin due to anthropogenic aerosol emissions, with values of above 0.65 in summer. In autumn and winter, AOD values over East Asia were lower, reduced to 0.25 over the TD and the GD.

The WRF-Chem model can reproduce spatial distributions and seasonal variations in aerosols over East Asia well. Dust aerosols contributed more than 95% of the total AOD over the TD and the GD. The simulated AOD over the TD was slightly higher than that from satellite retrievals, particularly in summer. The results of Chen et al. (2013, 2014a) also showed that the WRF-Chem model can capture the annual and seasonal variation in dust aerosols well over the TD and the GD. The TD dust was slightly overestimated in summer and autumn due to uncertainties in the seasonal variation in potential dust source regions used in the GOCART dust scheme. The MISR AOD is higher than that of the WRF-Chem simulations in the southwest of the domain, indicating that the model underestimates the emissions of anthropogenic aerosols in Northern India. In general, the simulation results capture the spatial and temporal distributions of both meteorological fields and

dust aerosols over East Asia well, providing confidence in the following discussions.

### 3.2 Dust Emissions over the TD and the GD

The differences in dust emissions over the TD and the GD in different seasons from 2007 to 2011 are shown in Table 1. Dust emissions over the TD and the GD reached maximum values in spring of 70.53 and 64.87 Tg yr<sup>-1</sup>, respectively, accounting for approximately 38.9% and 35.8%, respectively, of the total dust emissions over East Asia (Table 1). The most significant differences in dust emissions over the TD and GD were found in summer. The magnitude of dust emissions over the TD was 58.75 and 40.68 Tg yr<sup>-1</sup> over the GD. Dust emissions from these two major deserts in autumn and winter were substantially lower, reduced to 20–40 Tg yr<sup>-1</sup>. Figure 5 shows the proportion of dust emissions over the TD and the GD in different seasons, indicating that dust emissions over the TD and the GD are highest in spring, contributing 69% and 59%, respectively, to the annual total. There were significant seasonal differences in dust emissions over the TD, in particular between spring/summer and autumn/winter. Compared with the TD, the GD dust emissions exhibited a relatively homogeneous distribution across the different seasons, with a minimum in autumn, contributing approximately 20% to the annual dust emissions (Figure 5). The spatial distribution of dust concentrations over East Asia was similar to that of dust emissions. The TD dust concentrations were the highest and the average was approximately 0.8 mg m<sup>-3</sup>, while the GD dust is approximately 0.6 mg m<sup>-3</sup> in spring and summer. Dust concentrations over the GD in autumn and winter were greater than those over the TD, with maximum values of up to 1.1 mg m<sup>-3</sup> (Figure 6).

Dust emissions only reflect the efficiency of dust uplifting, and as such, it is not clear whether the greater dust emissions over the TD were accompanied by a greater contribution to dust concentrations over East Asia. Figure 7 shows the monthly dust concentrations at a height of 3–10 km (Figure 7a) and the ratio of dust concentrations at 3–10 km to below 3 km from 2007 to 2011 (Figure 7b). The inter-annual variations in dust concentrations over dust source regions were not significant (Figure 7a). Dust concentrations over the TD were generally higher than those over the GD between 3 and 10 km, particularly in spring and early autumn (mainly from March to September). It is worth noting that the ratio of the GD dust loadings at 3–10 km to below 3 km was greater than the ratio for the TD dust, although the GD dust emissions were smaller (Figure 7b). Compared with the TD, the GD region favors the uplift of dust particles to higher altitudes, particularly in summer (up to approximately 80%). There were similar dust concentrations at a height of 8–10 km over the TD and the GD (Figure 8). The ratio of dust concentrations at 8–10 km to below 3 km over the GD can reach up to 11%.

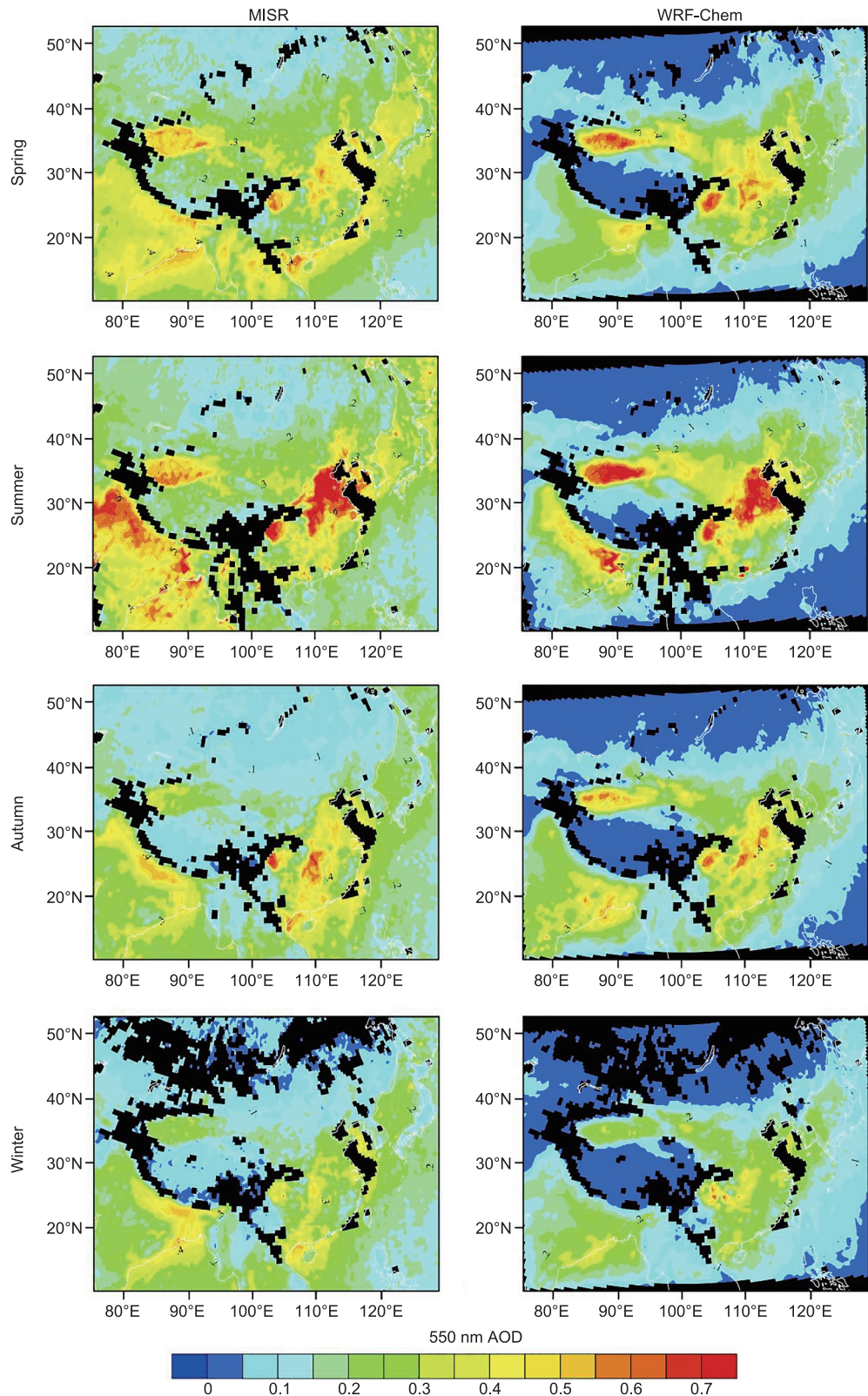


**Figure 4** Seasonal average AOD in 2007–2011 over East Asia from MISR retrievals (left) and WRF-Chem simulations (right).

Therefore, there were inconsistencies between dust emissions and dust concentrations over dust source regions, particularly in summer. Although the GD dust emissions were smaller, the

uplift of dust particles to higher altitudes (above 3 km) was more likely.

We further investigated the vertical structure in dust

**Table 1** Seasonal average dust emissions in the TD and the GD from 2007 to 2011<sup>a</sup>

|        | Taklimakan Desert ( $\text{Tg yr}^{-1}$ ) | Gobi Desert ( $\text{Tg yr}^{-1}$ ) |
|--------|---|-------------------------------------|
| Spring | 70.54 (38.9%)                             | 64.87 (35.8%)                       |
| Summer | 58.76 (41.8%)                             | 40.68 (28.9%)                       |
| Autumn | 33.34 (33.2%)                             | 36.13 (35.9%)                       |
| Winter | 24.67 (26.0%)                             | 38.02 (40.1%)                       |

<sup>a</sup> Bracketed values represent the contributions of dust emissions in the TD and the GD to the entirety of East Asia

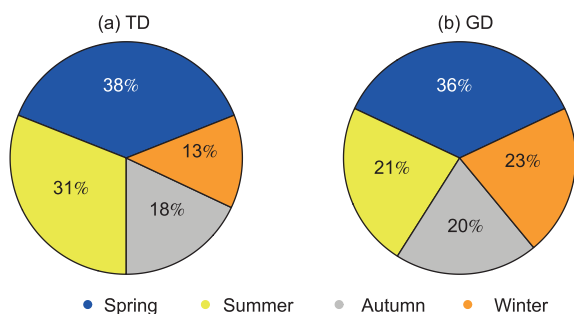


**Figure 5** Proportions of dust emission flux in the TD and the GD in different seasons during 2007–2011.

concentrations and potential temperatures over the TD and the GD in different seasons (Figure 9). Dust aerosols in these dust source regions generally accumulated below a height of 5 km, and peaked to more than  $400 \mu\text{g m}^{-3}$  below 1.5 km. Dust concentrations decreased rapidly with height

up to 9 km. Considering the relatively dense potential temperature contours, the TD was an obvious heat source, indicating that temperatures increased with vertical height due to the thermal effect, the atmospheric stratification was more stable, and the dust layer was mainly confined between 272 and 284 K in spring. Compared with the TD, dust concentrations below 3 km over the GD were lower approximately  $350 \mu\text{g m}^{-3}$ . However, the dust concentrations above 4 km over both the TD and GD were significant. Surface temperatures were inhomogeneous over the GD, particularly in summer, and the atmospheric baroclinicity favored the generation of southward thermal winds. In comparison, the potential temperature contours of the GD were relatively sparse, the temperature gradient was small, the vertical mixing was intense, and thermal turbulence development was strong, all of which favored the uplift of dust particles to higher altitudes and the dust layer was mainly confined between 280 and 292 K. Cross sections of zonal winds and wind vectors in the area of  $42^\circ\text{N}$ ,  $75.3^\circ\text{--}120.2^\circ\text{E}$  during different seasons in 2007–2011 are shown in Figure 10. The TD is located in the Tarim Basin and surrounded by mountains on three sides. Furthermore, the dominant surface wind direction was eastward. As a result, the TD dust particles were not easily transported outside of the Tarim Basin, such that most of the dust particles were re-deposited following uplift. Over the GD, the topography is relatively flat, with a high elevation. At heights of 9–15 km that region is influenced by two jet streams, resulting in high wind speeds in the upper

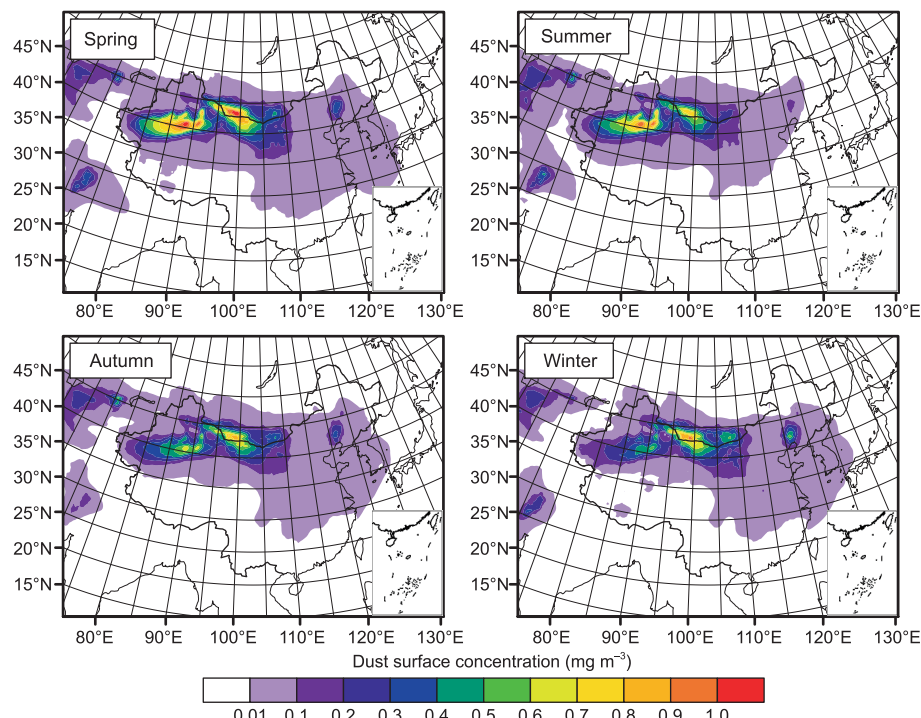


**Figure 6** The spatial distribution of near surface dust concentrations in different seasons over East Asia during 2007–2011.

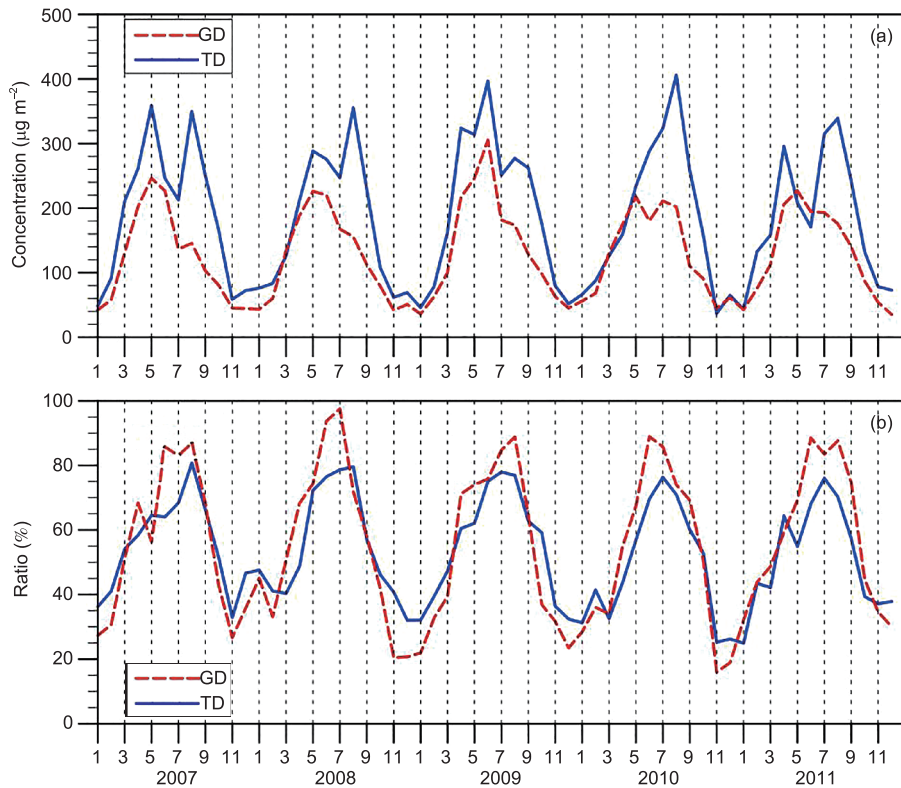


**Figure 7** The monthly average dust concentrations over the TD (blue solid line) and the GD (red dashed line) at 3–10 km altitude during 2007–2011 (a); the ratio of dust concentrations at 3–10 km to below 3 km over the TD and the GD during 2007–2011 (b).

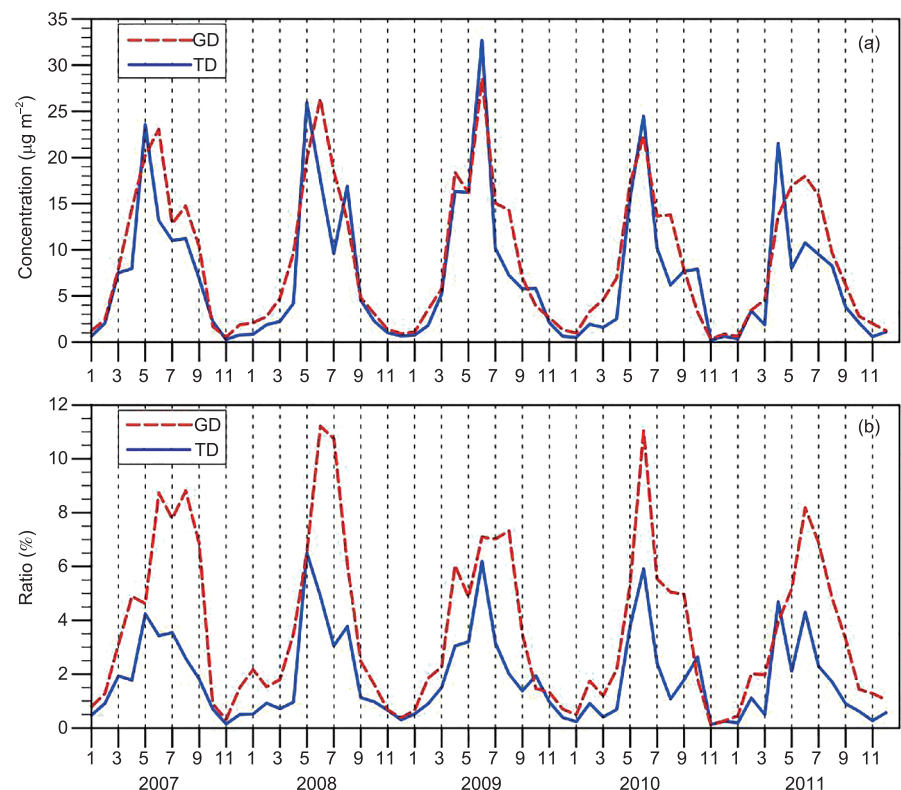


**Figure 8** The monthly average dust concentrations over the TD (blue solid line) and the GD (red dashed line) at 8–10 km altitude during 2007–2011 (a); the ratio of dust concentrations at 8–10 km to below 3 km over the TD and the GD during 2007–2011 (b).

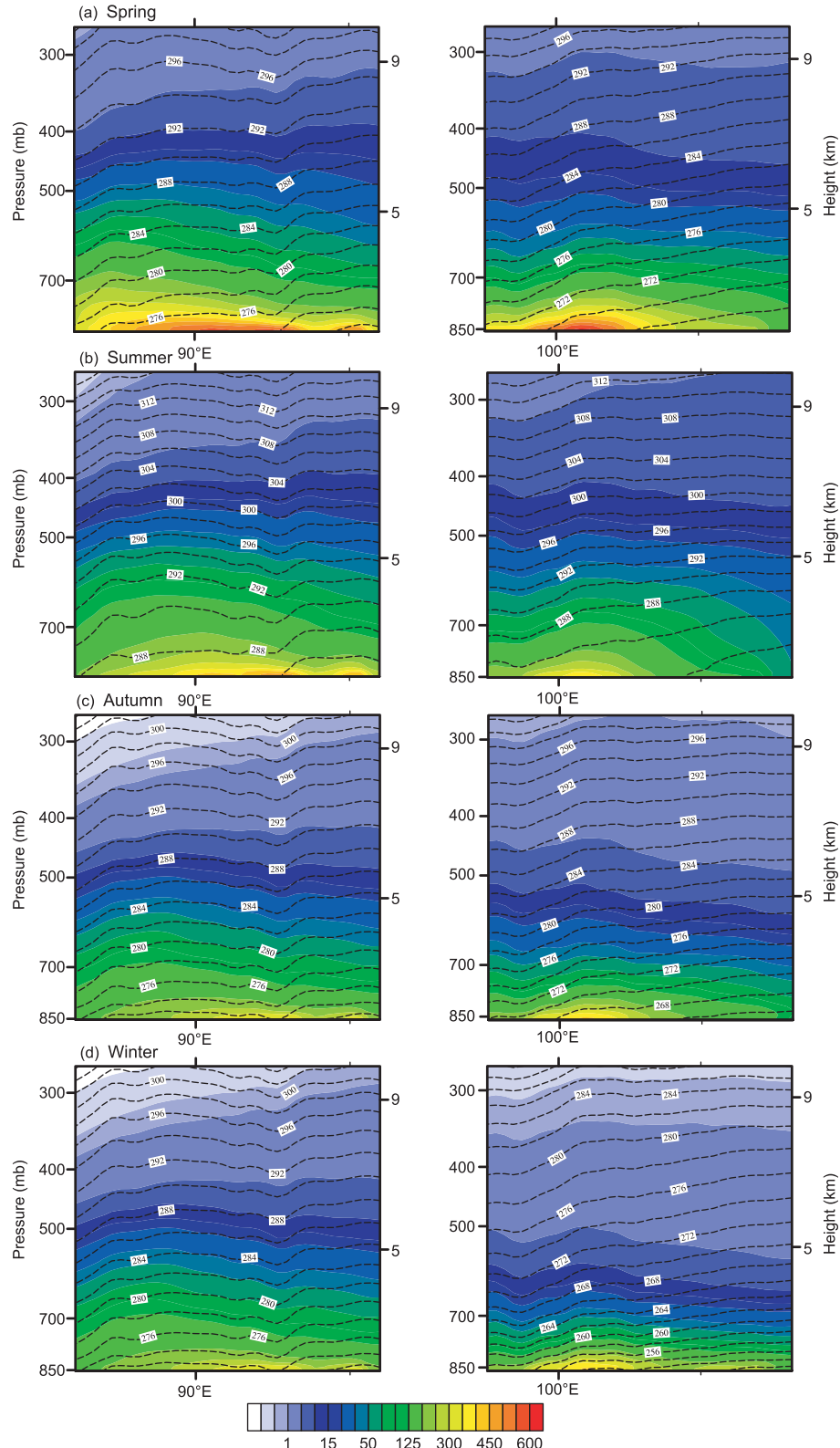


**Figure 9** The vertical distribution of zonal average dust concentrations (color scale,  $\mu\text{g m}^{-3}$ ) and potential temperatures (dotted line, K) over the TD (left) and the GD (right) in different seasons in 2007–2011.

air atmosphere. Deep convective mixing enabled the descending branch of jet streams to continuously transport momentum downward to the mid-troposphere, leading to en-

hanced wind speeds in the lower troposphere over the GD, which favored the uplift of the GD dust particles. Therefore, although the GD dust emissions were relatively small,

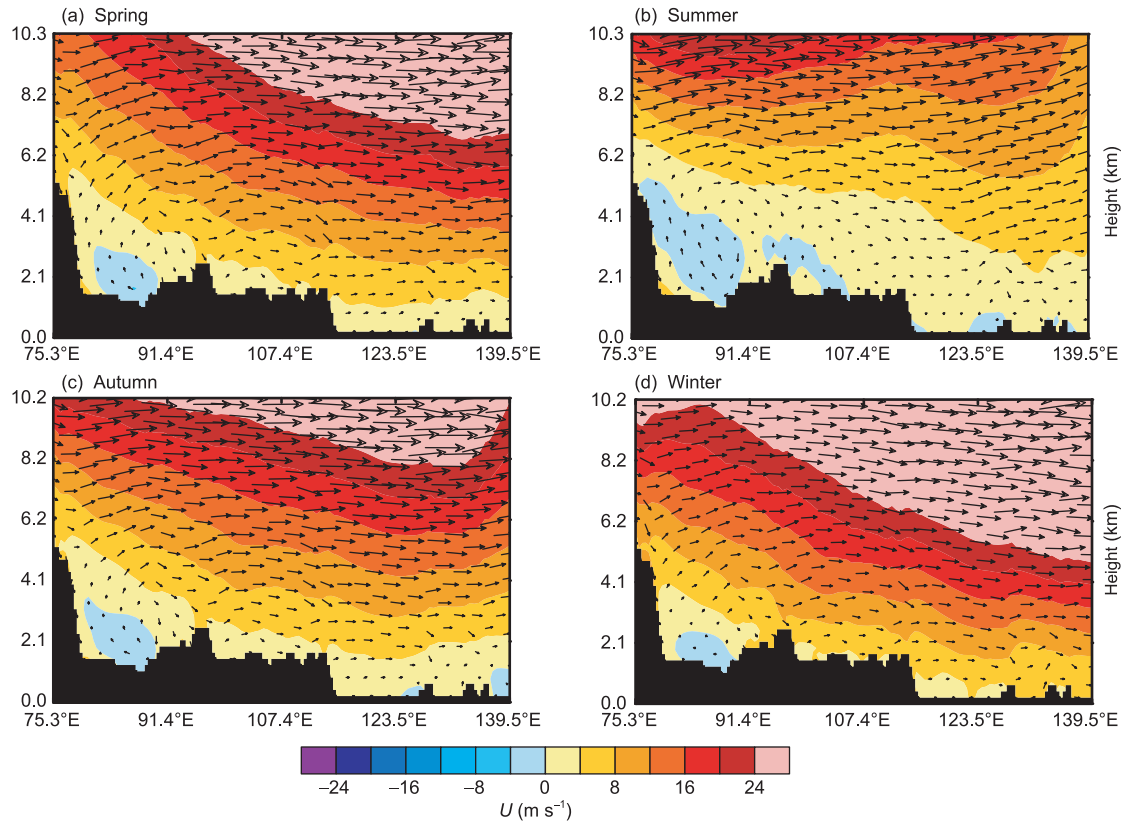


**Figure 10** Cross sections of the zonal wind and wind vector (vertical wind scaled by 100) in the area of  $42^{\circ}\text{N}$ ,  $75.3^{\circ}\text{--}120.2^{\circ}\text{E}$  in different seasons in 2007–2011.

the dust was more likely to be transported under the effects of strong westerly jets, such that the GD dust was the most important contributor to dust concentrations in East Asia as a whole.

### 3.3 Dust transport over the TD and GD

Dust emissions are a key factor in the dust cycle. Although dust emission fluxes in dust source regions can represent dust emission capabilities, the relationship between dust emissions in dust source regions and dust concentrations in deposition regions is nonlinear, due to the complexity of dust transport and deposition processes. Therefore, it is necessary to compare and analyze dust transport over the TD and the GD to investigate the contributions of these two dust source regions to East Asian dust concentrations. The seasonal average contributions of dust emissions and transport over the TD and the GD to the dust mass balance over East Asia in 2007–2011, based on the WRF-Chem model results, are shown in Figure 11. Here, the positive values denote the positive contributions and the negative values denote the negative contributions to the dust mass balance in the study area. In generally, the contributions of the GD dust to concentrations over East Asia were greater than those of the TD dust. The negative contributions of dust transport to the dust mass balance reached its maximum

in the GD ( $-24.8 \text{ g}(\text{m}^2\text{season})^{-1}$ ) in spring, accounting for 35.1% of dust emissions, while the contributions of the TD dust transport only accounted for 25.4%. Han et al. (2004) simulated the long-range transport of East Asian dust in the spring of 2002 and found that about 23% of dust particles over these two major dust source regions were suspended in the air or transported over a long distance, which is in agreement with the results of this study. In summer, the dust emission flux over the TD was  $54.3 \text{ g}(\text{m}^2\text{season})^{-1}$ , which was greater than that over the GD ( $45.3 \text{ g}(\text{m}^2\text{season})^{-1}$ ). However, dust transport fluxes in the TD and the GD were virtually the same, around  $-14 \text{ g}(\text{m}^2\text{season})^{-1}$ , indicating that transport of the GD dust was more efficient than that of the TD dust. Dust transport fluxes in the GD at approximately  $-11 \text{ g}(\text{m}^2\text{season})^{-1}$  were also greater than those in the TD in autumn and winter.

To gain a better understanding of the dust transport in the TD and the GD, Figure 12 shows the spatial distribution of dust transport fluxes over East Asia in different seasons during 2007–2011. The area between  $30^{\circ}\text{N}$  and  $45^{\circ}\text{N}$ , which includes northern China, Japan and Korea, is influenced by two dust sources. The dust transport flux of the GD was significantly larger than that of the TD in spring, with high values extending southeast to the Beijing-Tianjin-Hebei region (approximately  $250 \text{ g}(\text{m}^2\text{season})^{-1}$ ). Compared with spring, dust transport in summer was weaker with peak values of the dust

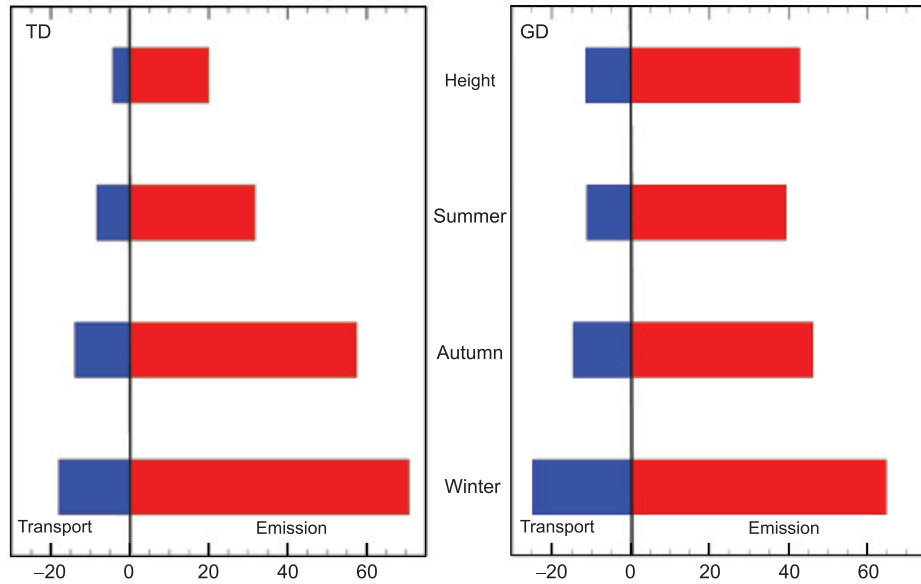


**Figure 11** Seasonal average contributions of dust emissions and transport over the TD and the GD to the dust mass balance over East Asia in 2007–2011 based on the WRF-Chem model. For dust budget analysis, the positive values denote positive contributions and the negative values denote the negative contributions to the dust mass balance in the study area. Units:  $\text{g}(\text{m}^2 \text{season})^{-1}$ .

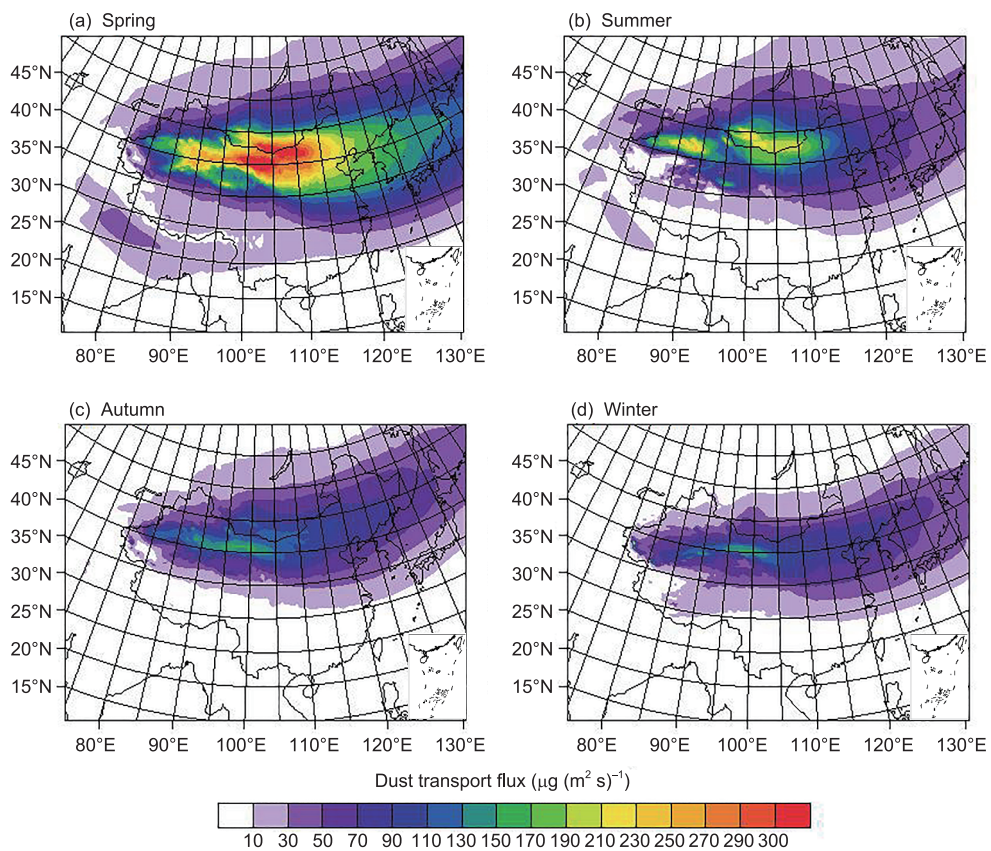


**Figure 12** The spatial distribution of dust transport flux over East Asia in different seasons in 2007–2011. Unit:  $\mu\text{g}(\text{m}^2 \text{s})^{-1}$ .

transport flux decreasing to  $200 \text{ g}(\text{m}^2 \text{s})^{-1}$ , and the dust transport flux to the Beijing-Tianjin-Hebei region was approximately  $100 \text{ g}(\text{m}^2 \text{s})^{-1}$ . The dust transport flux was even lower in autumn and winter, but the GD dust still showed strong

transport towards the southeast, with a dust transport flux of up to  $170 \text{ g}(\text{m}^2 \text{s})^{-1}$ . The main reasons for the divergences in dust transport between the TD and GD are shown in Figures 9 and 10. It is difficult for the TD dust to be transported af-

ter uplift due to the obstruction by surrounding mountains, and low wind speeds in the upper atmosphere. Long-range transport was only possible when the TD dust particles were uplifted above 4 km and entrained in westerlies. The surface wind speeds in the GD were relatively small, and the dominant wind direction at 10 m was westward or northwestward. Two jet streams converge over the GD, with wind speeds reaching above  $20 \text{ ms}^{-1}$  at a height of 500 hPa in spring and winter. In addition, cold air frequently influences the GD region along the northwest or north path, which also produces wind gusts at regional scales (Zhang B et al., 2008). As a result, although the dust emissions are smaller in the GD, the GD dust can be uplifted to higher altitudes under the impact of strong vertical mixing, and then can then be transported to the southeast or northeast. Thus, the GD dust was the most important contributor to dust concentrations over distant areas such as Beijing-Tianjin-Hebei region, and even over the entirety of East Asia. It is worth noting that the westerly jet shift to the north of the TP in summer (up to  $44^\circ\text{N}$ ) (Zhang Y C et al., 2008), leading to a weaker eastward dust transport. Therefore, the TD dust particles were easily transported southward and further uplifted to the northern slopes of the TP (Huang et al., 2007; Chen et al., 2013, 2014b).

It is undeniable that, because of the impact of westerlies, the long-range transport of the TD dust inevitably results in contributions to dust concentrations over the GD. To investigate how much dust concentrations in the GD was transported from the TD, the vertical distributions of dust outflux to the east of the TD and GD (the right side of the two red boxes in Figure 1) are shown in Figure 13. The red solid line represents the differences in eastward dust outflux from the GD and the TD. The eastward dust outflux over the GD was higher than that over the TD with an obvious high value zone at 2 km (approximately  $478 \mu\text{g s}^{-1}$ ). Figure 13 indicates that although some of the dust in the GD was contributed by the TD, the GD still showed very strong dust transport capabilities in spring, which was particularly apparent in the lower troposphere (2–4 km). Similarly, there was a clear high value zone at 2 km for the eastward dust outflux over the GD in autumn and winter. In particular, the outflux of the GD dust was greater than that of the TD dust at 2–4 km height. The magnitudes of the dust outflux in the GD and the TD were consistent above 4 km, because most dust particles in this altitude bin in the GD were transported from the TD, via the westerly jet. However, the magnitudes of the dust outflux in this altitude bin were much smaller at lower altitudes. According to the distribution pattern and the values of the dust transport flux over the TD and the GD, as shown in Figure 12, the TD dust could only be transported over long distances only when it was uplifted above 4 km, and the dust transport flux at this level was relatively small (approximately  $124 \mu\text{g s}^{-1}$  in spring). The GD dust was more likely to be transported below 4 km and thus made larger contributions to dust concen-

trations over inland East Asia.

### 3.4 Dry and wet deposition of dust over the TD and GD

Dust deposition processes are divided into dry and wet deposition. Dry deposition of dust is directly related to dust emissions (Figure 14) and is more important than wet deposition. The seasonal dry deposition was approximately  $10\text{--}60 \text{ g m}^{-2}$  over the TD and GD. The magnitude of dry deposition in spring and summer was greater than that in autumn and winter. Two distinct high value centers of dry deposition, up to  $50 \text{ g m}^{-2}$ , were located in the TD and the GD in spring (Figure 14). In autumn and winter, dry deposition mainly occurred in the GD (approximately  $10\text{--}20 \text{ g m}^{-2}$ ) and was associated with strong dust emissions. Wet deposition of dust is mainly determined by dust concentrations and precipitation at regional scales. The highest value of dust wet deposition was located in the TD, mainly in spring and summer (Figure 15). The magnitude of wet deposition was greatest in spring and summer at approximately  $4 \text{ g m}^{-2}$ , which is only one tenth of the dry deposition, followed by autumn ( $1.5 \text{ g m}^{-2}$ ), and lastly winter ( $0.6 \text{ g m}^{-2}$ ). Wet deposition of dust over the GD was much lower than that over the TD. Wet deposition of the GD dust was approximately  $2 \text{ g m}^{-2}$  in spring and summer, while it was close to zero in winter due to the lack of precipitation. The simulation results of Han et al. (2004) also found that compared with wet deposition, dry deposition was the dominant sink of dust in dust source regions and remote areas over East Asia. Approximately 71% of dust particles were re-deposited to the surface through dry deposition processes, and the contribution of wet deposition processes were only 6%. In addition, the deposition efficiency of coarse particles ( $>2 \mu\text{m}$ ) was more significant.

## 4. Conclusions

The WRF-Chem model, a state-of-art air quality model, was used to investigate dust emissions, transport and deposition over the Taklimakan Desert (TD) and the Gobi Desert (GD) in 2007–2011. Results showed that the WRF-Chem model could reproduce the spatial and seasonal distributions of dust aerosols in the TD and the GD well. However, the magnitude of the simulated TD dust concentrations were slightly higher than those from satellite retrievals in summer and autumn because of uncertainties in seasonal variation in potential dust source regions used in the dust emission scheme. The dynamic land cover needs to be considered in the dust emission scheme in the future. Overall, the ability of the WRF-Chem model to capture the observed optical and radiative dust properties over East Asia provides confidence in future investigations of dust emissions, transport and deposition over the TD and the GD. Emissions, uplift, and long-range transport of dust over the TD and the GD are quite different due to dif-

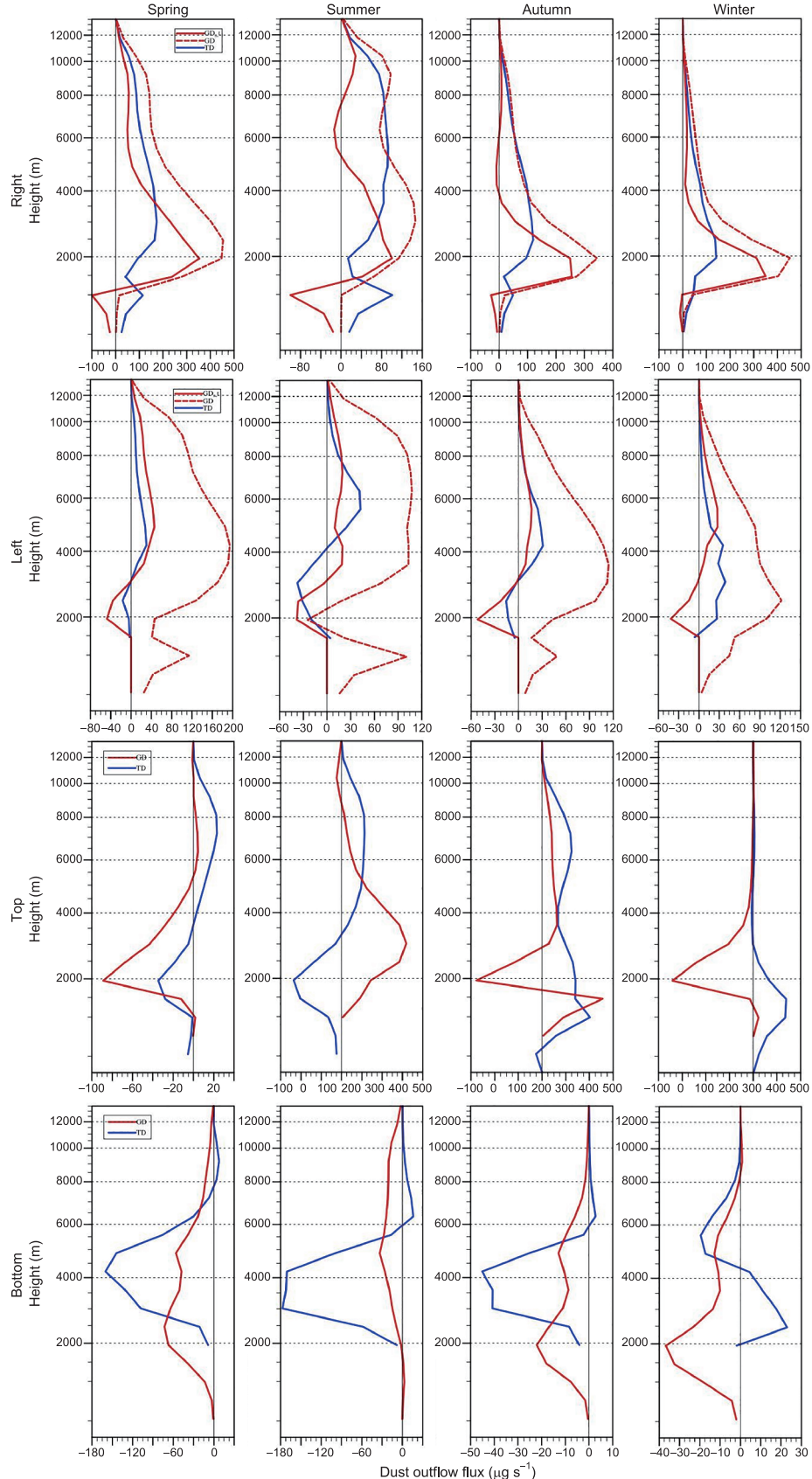


**Figure 13** The vertical distribution of dust outflux to the east of the TD (blue solid line) and the GD (red dashed line) (the right side of two red boxes in Figure 1) in 2007–2011. The red solid line represents the differences in eastward dust outflux between the GD and the TD. Unit:  $\mu\text{g s}^{-1}$ .

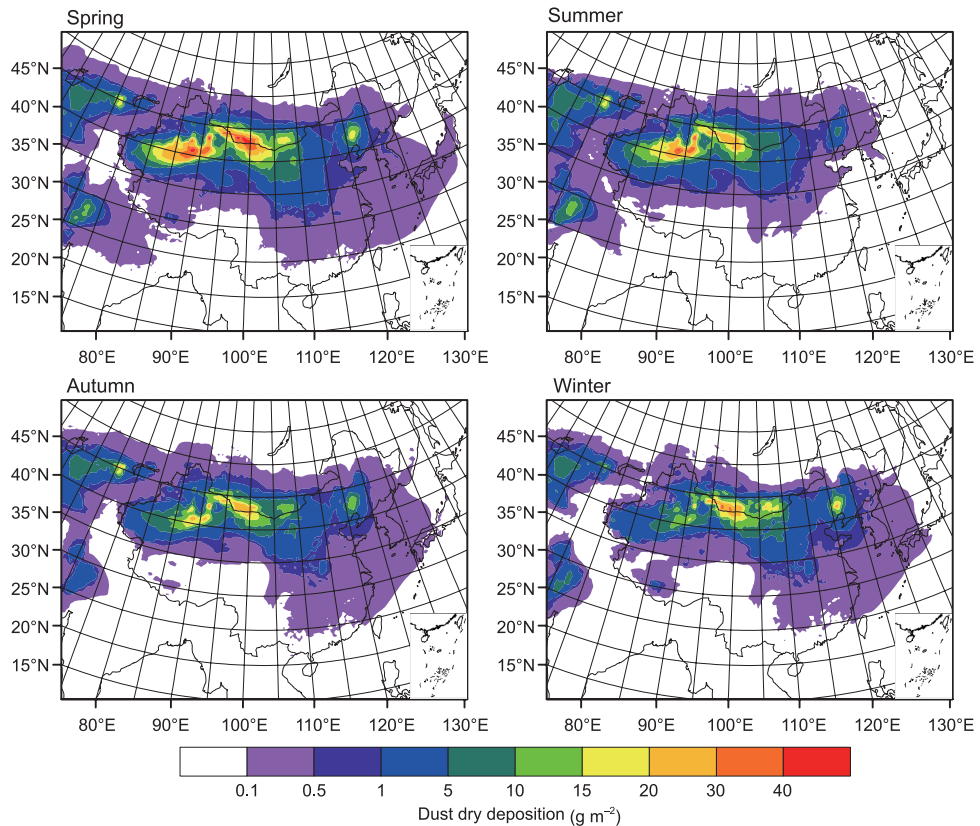


**Figure 14** The spatial distribution of dry deposition of dust (unit:  $\text{gm}^{-2}$ ) over East Asia in 2007–2011 based on the WRF-Chem model.

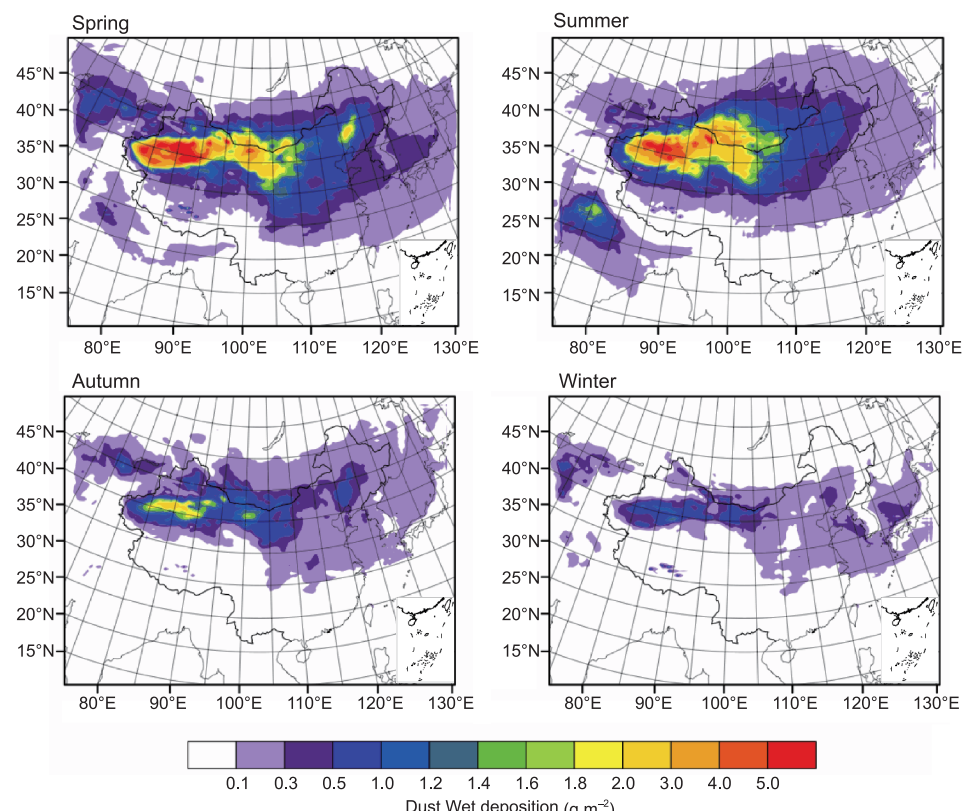


**Figure 15** The spatial distribution of wet deposition of dust over East Asia in 2007–2011 based on the WRF-Chem model.

ferences in topography, elevation, thermal conditions, and atmospheric circulation. This work emphasizes the importance of the contributions of GD dust to East Asia as a whole. The main findings are as follows:

(1) Dust emissions. The TD and GD are the two main dust source regions in East Asia. The efficiency of dust uplift over the TD was significantly higher than over the GD such that the TD is the largest dust source region in East Asia. The dust emission flux was  $70.54 \text{ Tg yr}^{-1}$ , accounting for 42% of the total dust emissions over East Asia in spring. Dust emissions over the GD were lower than over the TD. Differences in dust uplift efficiency between the TD and the GD were most obvious in summer, up to  $18 \text{ Tg yr}^{-1}$ .

(2) Dust transport. There was a particular inconsistency between the dust emissions and transport in the TD and the GD. The ratio of the GD dust concentrations at heights of 3–10 km to below 3 km reached up to 11%. Dust emissions in the TD were stronger than those in the GD, but the GD favored uplifting of dust to relatively high altitudes, particularly in summer. Approximately 25% and 35% of dust aerosols in the TD and the GD, respectively, were transported to remote areas over East Asia in spring. Deep convective mixing enabled the descending branch of jet streams to continuously transport momentum downward to the mid-troposphere, leading to enhanced wind speeds in the lower troposphere over the GD. The dust was likely transported under the effects of strong westerly jets with frequent cold air systems from the west, north-west, and north playing the most important role in contributions to dust concentrations over East Asia as a whole. The TD is surrounded by mountains on three sides, where the surface wind was dominated by easterly wind with low wind speeds at high altitudes. As a result, the TD dust particles were not easily transported outside the Tarim Basin. Most dust particles over the TD were re-deposited after uplift. It is only when the TD dust particles are uplifted above 4 km and entrained in westerlies that they begin to be transported over long distances.

(3) Dust deposition. Dry deposition is the dominant sink of dust in dust source regions, with the peak values of up to  $50 \text{ g m}^{-2}$ . Wet deposition of dust mainly depends on precipitation and dust concentrations. In spring and summer, the magnitude of wet deposition in dust source regions was approximately  $4 \text{ g m}^{-2}$ , which is only one-tenth of the dry deposition. The dry and wet deposition of dust was similar at  $1\text{--}5 \text{ g m}^{-2}$  because of the sufficient precipitation.

Next, we will provide further quantitative estimates of the climate effects of the TD and GD dust in different seasons over East Asia, based on the WRF-Chem model used in this study.

**Acknowledgements** We acknowledge Chun Zhao and Yun Qian for their help for this work. This research was supported by the National Natural Science Foundation of China (Grant No. 41405003), Innovative Re-

search Groups of the National Natural Science Foundation of China (Grant No. 41521004), and the Programme of Introducing Talents of Discipline to Universities (Grant No. B13045) and the Foundation of Key Laboratory for Semi-Arid Climate Change of the Ministry of Education in Lanzhou University.

## References

- Belly P Y. 1964. Sand movement by wind. US Army Coastal Eng Res Tech Memo, 1–38
- Cavazos-Guerra C, Todd M C. 2012. Model simulations of complex dust emissions over the Sahara during the West African monsoon onset. *Adv Meteor*, 2012: 1–17
- Chen F, Dudhia J. 2001. Coupling an advanced land surface-hydrology model with the Penn State-NCAR MM5 modeling system. Part I: Model implementation and sensitivity. *Mon Weather Rev*, 129: 569–585
- Chen S Y, Huang J P, Kang L T, Wang H, Ma X, He Y, Yuan T, Yang B, Huang Z, Zhang G. 2017. Emission, transport, and radiative effects of mineral dust from the Taklimakan and Gobi Deserts: Comparison of measurements and model results. *Atmos Chem Phys*, 17: 2401–2421
- Chen S Y, Huang J P, Qian Y, Ge J M, Su J. 2014a. Effects of aerosols on autumn precipitation over Mid-eastern China. *J Trop Meteorol*, 20: 242–250
- Chen S Y, Huang J P, Zhao C, Qian Y, Leung L R, Yang B. 2013. Modeling the transport and radiative forcing of Taklimakan dust over the Tibetan Plateau: A case study in the summer of 2006. *J Geophys Res-Atmos*, 118: 797–812
- Chen S Y, Zhao C, Qian Y, Leung L R, Huang J P, Huang Z W, Bi J R, Zhang W, Shi J S, Yang L, Li D S, Li J X. 2014b. Regional modeling of dust mass balance and radiative forcing over East Asia using WRF-Chem. *Aeolian Res*, 15: 15–30
- Cheng T, Chen H, Gu X, Yu T, Guo J, Guo H. 2012. The inter-comparison of MODIS, MISR and GOCART aerosol products against AERONET data over China. *J Quant Spectrosc Ra*, 113: 2135–2145
- Diner D J, Hodos R A, Davis A B, Garay M J, Martonchik J V, Sanghavi S V, von Allmen P, Kokhanovsky A A, Zhai P. 2012. An optimization approach for aerosol retrievals using simulated MISR radiances. *Atmos Res*, 116: 1–14
- Diner D J, Martonchik J V, Kahn R A, Pinty B, Gobron N, Nelson D L, Holben B N. 2005. Using angular and spectral shape similarity constraints to improve MISR aerosol and surface retrievals over land. *Remote Sens Environ*, 94: 155–171
- Eguchi K, Uno I, Yumimoto K, Takemura T, Shimizu A, Sugimoto N, Liu Z. 2009. Trans-pacific dust transport: Integrated analysis of NASA/CALIPSO and a global aerosol transport model. *Atmos Chem Phys*, 9: 3137–3145
- Fast J D, Gustafson Jr. W I, Easter R C, Zaveri R A, Barnard J C, Chapman E G, Grell G A, Peckham S E. 2006. Evolution of ozone, particulates, and aerosol direct radiative forcing in the vicinity of Houston using a fully coupled Meteorology-Chemistry-Aerosol Model. *J Geophys Res*, 111: D21305
- Fu Q, Thorsen T J, Su J, Ge J M, Huang J P. 2009. Test of Mie-based single-scattering properties of non-spherical dust aerosols in radiative flux calculations. *J Quant Spectrosc Ra*, 110: 1640–1653
- Ge J M, Huang J P, Xu C P, Qi Y L, Liu H Y. 2014. Characteristics of Taklimakan dust emission and distribution: A satellite and reanalysis field perspective. *J Geophys Res-Atmos*, 119: 11772–11783
- Ge J M, Su J, Ackerman T P, Fu Q, Huang J P, Shi J S. 2010. Dust aerosol optical properties retrieval and radiative forcing over northwestern China during the 2008 China-U.S. joint field experiment. *J Geophys Res*, 115: D00K12
- Grell G A, Peckham S E, Schmitz R, McKeen S A, Frost G, Skamarock W C, Eder B. 2005. Fully coupled “online” chemistry within the WRF model. *Atmos Environ*, 39: 6957–6975

- Ginoux P, Chin M, Tegen I, Prospero J M, Holben B, Dubovik O, Lin S J. 2001. Sources and distributions of dust aerosols simulated with the GOCART model. *J Geophys Res*, 106: 20255–20273
- Ginoux P, Prospero J, Torres O, Chin M. 2004. Long-term simulation of global dust distribution with the GOCART model: Correlation with North Atlantic oscillation. *Environ Model Softw*, 19: 113–128
- Gong S L, Zhang X Y, Zhao T L, McKendry I G, Jaffe D A, Lu N M. 2003. Characterization of soil dust aerosol in China and its transport and distribution during 2001 ACE-Asia: 2. Model simulation and validation. *J Geophys Res*, 108: 4262
- Han Z, Ueda H, Matsuda K, Zhang R, Arao K, Kanai Y, Hasome H. 2004. Model study on particle size segregation and deposition during Asian dust events in March 2002. *J Geophys Res*, 109: D19205
- Hong S Y, Noh Y, Dudhia J. 2006. A new vertical diffusion package with an explicit treatment of entrainment processes. *Mon Weather Rev*, 134: 2318–2341
- Huang J P, Fu Q, Su J, Tang Q, Minnis P, Hu Y, Yi Y, Zhao Q. 2009. Taklimakan dust aerosol radiative heating derived from CALIPSO observations using the Fu-Liou radiation model with CERES constraints. *Atmos Chem Phys*, 9: 4011–4021
- Huang J P, Fu Q, Zhang W C, Wang X, Zhang R, Ye H, Warren S G. 2011. Dust and black carbon in seasonal snow across northern China. *Bull Amer Meteorol Soc*, 92: 175–181
- Huang J P, Guan X, Ji F. 2012. Enhanced cold-season warming in semi-arid regions. *Atmos Chem Phys*, 12: 5391–5398
- Huang J P, Lin B, Minnis P, Wang T, Wang X, Hu Y, Yi Y, Ayers J K. 2006a. Satellite-based assessment of possible dust aerosols semi-direct effect on cloud water path over East Asia. *Geophys Res Lett*, 33: L19802
- Huang J P, Minnis P, Chen B, Huang Z, Liu Z, Zhao Q, Yi Y, Ayers J K. 2008. Long-range transport and vertical structure of Asian dust from CALIPSO and surface measurements during PACDEX. *J Geophys Res*, 113: D23212
- Huang J P, Minnis P, Lin B, Wang T, Yi Y, Hu Y, Sun-Mack S, Ayers K. 2006b. Possible influences of Asian dust aerosols on cloud properties and radiative forcing observed from MODIS and CERES. *Geophys Res Lett*, 33: L06824
- Huang J P, Minnis P, Yi Y, Tang Q, Wang X, Hu Y, Liu Z, Ayers K, Trepte C, Winker D. 2007. Summer dust aerosols detected from CALIPSO over the Tibetan Plateau. *Geophys Res Lett*, 34: L18805
- Huang J P, Wang T H, Wang W, Li Z, Yan H. 2014. Climate effects of dust aerosols over East Asian arid and semiarid regions. *J Geophys Res Atmos*, 119: 11,398–11,416
- Huang Z W, Huang J P, Bi J R, Wang G Y, Wang W C, Fu Q, Li Z Q, Tsay S C, Shi J S. 2010. Dust aerosol vertical structure measurements using three MPL lidars during 2008 China-U.S. joint dust field experiment. *J Geophys Res*, 115: D00K15
- Huneeus N, Schulz M, Balkanski Y, Griesfeller J, Kinne S, Prospero J, Bauer S, Boucher O, Chin M, Dentener F, Diehl T, Easter R, Fillmore D, Ghan S, Ginoux P, Grini A, Horowitz L, Koch D, Krol M C, Landing W, Liu X, Mahowald N, Miller R, Morcrette J J, Myhre G, Penner J E, Perlitz J, Stier P, Takemura T, Zender C. 2010. Global dust model intercomparison in AeroCom phase I. *Atmos Chem Phys Discuss*, 10: 23781–23864
- Jia R, Liu Y Z, Chen B, Zhang Z J, Huang J P. 2015. Source and transportation of summer dust over the Tibetan Plateau. *Atmos Environ*, 123: 210–219
- Kahn R A, Gaitley B J. 2015. An analysis of global aerosol type as retrieved by MISR. *J Geophys Res-Atmos*, 120: 4248–4281
- Kain J S. 2004. The kain-fritsch convective parameterization: An update. *J Appl Meteorol*, 43: 170–181
- Canayama S, Yabuki S, Zeng F L, Liu M Z, Shen Z B, Liu L C, Yanagisawa F, Abe O. 2005. Size-dependent geochemical characteristics of Asian dust. *J Meteorol Soc Jpn*, 83A: 107–120
- Kang L T, Chen S Y. 2017. Numerical modeling study of a dust storm process in Northern China (in Chinese). *Atoms Environ*, 37: 321–331
- Kang L T, Huang J P, Chen S Y, Wang X. 2016. Long-term trends of dust events over Tibetan Plateau during 1961–2010. *Atmos Environ*, 125: 188–198
- Kim J. 2008. Transport routes and source regions of Asian dust observed in Korea during the past 40 years (1965–2004). *Atmos Environ*, 42: 4778–4789
- Marticorena B, Bergametti G. 1995. Modeling the atmospheric dust cycle: 1. Design of a soil-derived dust emission scheme. *J Geophys Res*, 100: 16415
- Martonchik J V, Diner D J, Crean K A, Bull M A. 2002. Regional aerosol retrieval results from MISR. *IEEE Trans Geosci Remote Sens*, 40: 1520–1531
- Martonchik J V, Diner D J, Kahn R, Gaitley B, Holben B N. 2004. Comparison of MISR and AERONET aerosol optical depths over desert sites. *Geophys Res Lett*, 31: L16102
- Morrison H, Curry J A, Khvorostyanov V I. 2005. A new double-moment microphysics parameterization for application in cloud and climate models. Part I: Description. *J Atmos Sci*, 62: 1665–1677
- Nakano T, Yokoo Y, Nishikawa M, Koyanagi H. 2004. Regional Sr-Nd isotopic ratios of soil minerals in northern China as Asian dust fingerprints. *Atmos Environ*, 38: 3061–3067
- Pye K. 1989. Aeolian Dust and Dust Deposites. 2nd ed. San Diego: Academic Press
- Qian Y, Gong D Y, Fan J W, Leung L R, Bennartz R, Chen D L, Wang W. 2009. Heavy pollution suppresses light rain in China: Observations and modeling. *J Geophys Res*, 114: D00K02
- Shao Y, Wyrwoll K H, Chappell A, Huang J, Lin Z, McTainsh G H, Mikami M, Tanaka T Y, Wang X, Yoon S. 2011. Dust cycle: An emerging core theme in Earth system science. *Aeolian Res*, 2: 181–204
- Shao Y P, Yang Y, Wang J J, Song Z X, Leslie L M, Dong C H, Zhang Z H, Lin Z H, Kanai Y, Yabuki S, Chun Y. 2003. Northeast Asian dust storms: Real-time numerical prediction and validation. *J Geophys Res*, 108: 4691–4710
- Shen Y B, Shen Z B, Du M Y. 2005. Factors affecting on dust emission by wind erosion and their variational characteristics (in Chinese). *Plateau Meteorol*, 24: 611–616
- Su J, J P , HuangQ , FuMinnis P, Ge J M, Bi J R. 2008. Estimation of Asian dust aerosol effect on cloud radiation forcing using Fu-Liou radiative model and CERES measurements. *Atmos Chem Phys*, 8: 2763–2771
- Sun J, Zhang M, Liu T. 2001. Spatial and temporal characteristics of dust storms in China and its surrounding regions, 1960–1999: Relations to source area and climate. *J Geophys Res*, 106: 10325–10333
- Tesfaye M, Sivakumar V, Botai J, Mengistu Tsidi G. 2011. Aerosol climatology over South Africa based on 10 years of Multiangle Imaging Spectroradiometer (MISR) data. *J Geophys Res*, 116: D20216
- Uno I, Yumimoto K, Shimizu A, Hara Y, Sugimoto N, Wang Z, Liu Z, Winker D M. 2008. 3D structure of Asian dust transport revealed by CALIPSO lidar and a 4DVAR dust model. *Geophys Res Lett*, 35: L06803
- Wang J, Xu X G, Henze D K, Zeng J, Ji Q, Tsay S C, Huang J P. 2012. Top-down estimate of dust emissions through integration of MODIS and MISR aerosol retrievals with the GEOS-Chem adjoint model. *Geophys Res Lett*, 39: L08802
- Wang Q Z, Zhuang G S, Huang K, Liu T N, Lin Y F, Deng C R, Fu Q, Fu J S, Chen J K, Zhang W J, Yiming M. 2016. Evolution of particulate sulfate and nitrate along the Asian dust pathway: Secondary transformation and primary pollutants via long-range transport. *Atmos Res*, 169: 86–95
- Wang X, Huang J P, Zhang R D, Chen B, Bi J R. 2010. Surface measurements of aerosol properties over northwest China during ARM China 2008 deployment. *J Geophys Res*, 115: D00K27
- Weaver C J, Ginoux P, Hsu N C, Chou M D, Joiner J. 2002. Radiative forcing of Saharan dust: GOCART model simulations compared with ERBE Data. *J Atmos Sci*, 59: 736–747
- Yue X, Wang H, Liao H, Fan K. 2010. Direct climatic effect of dust aerosols in the NCAR community atmosphere model version 3 (CAM3). *Adv*

- Atmos Sci, 27: 230–242
- Yue X, Liao H, Tang J P. 2013. Simulation of the direct radiative effect of mineral dust and sea salt aerosols in a doubled Carbon dioxide climate. *Atmos Ocean Sci Lett*, 6: 343–348
- Zender C S, Bian H, Newman D. 2003. Mineral Dust Entrainment and Deposition (DEAD) model: Description and 1990s dust climatology. *J Geophys Res*, 108: 4416
- Zhang B, Tsunekawa A, Tsubo M. 2008. Contributions of sandy lands and stony deserts to long-distance dust emission in China and Mongolia during 2000–2006. *Glob Planet Change*, 60: 487–504
- Zhang H, Wang Z, Guo P, Wang Z. 2009a. A modeling study of the effects of direct radiative forcing due to carbonaceous aerosol on the climate in East Asia. *Adv Atmos Sci*, 26: 57–66
- Zhang H, Ma J H, Zheng Y F. 2009b. A modeling study of global radiative forcing due to dust aerosol (in Chinese). *Acta Meteorol Sin*, 67: 510–521
- Zhang J, Reid J S. 2010. A decadal regional and global trend analysis of the aerosol optical depth using a data-assimilation grade over-water MODIS and Level 2 MISR aerosol products. *Atmos Chem Phys*, 10: 10949–10963
- Zhang X Y, Gong S L, Zhao T L, Arimoto R, Wang Y Q, Zhou Z J. 2003. Sources of Asian dust and role of climate change versus desertification in Asian dust emission. *Geophys Res Lett*, 30: 2272
- Zhang Y C, Takahashi M, Guo L. 2008. Analysis of the East Asian subtropical westerly jet simulated by CCSR/NIES/FRCGC coupled climate system model. *J Meteorol Soc Jpn*, 86: 257–278
- Zhao C, Chen S, Leung L R, Qian Y, Kok J F, Zaveri R A, Huang J. 2013. Uncertainty in modeling dust mass balance and radiative forcing from size parameterization. *Atmos Chem Phys*, 13: 10733–10753
- Zhao C S, Dabu X, Li Y. 2004. Relationship between climatic factors and dust storm frequency in Inner Mongolia of China. *Geophys Res Lett*, 31: L01103
- Zhao C, Liu X, Leung L R, Johnson B, McFarlane S A, Gustafson Jr. W I, Fast J D, Easter R. 2010. The spatial distribution of mineral dust and its shortwave radiative forcing over North Africa: Modeling sensitivities to dust emissions and aerosol size treatments. *Atmos Chem Phys*, 10: 8821–8838